Bachelorarbeit

Simulation and testing of a CO_2 cooling device for Belle II

Jo-Frederik Krohn

Datum der Abgabe: 06.02.2014

Erstgutachterin:

Prof. Dr. Caren Hagner

Institut für Experimentalphysik
Universität Hamburg

Zweitgutachter:

Dr. Carsten Niebuhr

Deutsches Elektronen-Synchrotron

Zusammenfassung

Im Rahmen dieser Arbeit wurde ein Experiment zur Untersuchung des CO_2 Kühlungssystems von Belle II durchgeführt. Insbesondere wurde dabei das thermische Mock up der inneren Detektoren auf seine Fähigkeit geprüft die anliegende Wärmelast abzuführen. Diese Information wurde aus Druckverlustmessungen gewonnen. Desweiteren wurde versucht die gemessenen Ergebnisse anhand von numerischen Simulationen zu reproduzieren, um mit diesen Rückschlüsse auf die stattfindenden physikalischen Prozesse machen zu können und Änderungen der experimentellen Geometrie darstellen zu können.
Diese Simulationen sind nicht in der Lage die gemessenen Ergebnisse zu reproduzieren. Eine Analyse der aufgetretenen Probleme und wurde durchgeführt.

Abstract

This assignment investigates two experiments that mimic the CO_2 cooling system of Belle II. The thermal mock up of the innermost detector systems were analysed for its ability to provide the necessary cooling. This was done using pressure drop measurements. Additionally, numerical simulations were performed in order to extend the knowledge of the inherent physical processes, and to be able to project changes in geometry. Theses simulations were not able to reproduce the measured data. An analysis of the problems occurred and possible solutions was conducted.

Contents

1. Introduction **1**

2. The Belle II Experiment **2**
2.1. The spectrometer 2
2.1.1. The Pixel Detector - PXD 3
2.1.2. The Support and Cooling Block - SCB 4
2.1.3. The Silicon Vertex Detector - SVD 5

3. Theory **7**
3.1. The 2-Phase State 7
3.2. Boiling 9
3.3. 2-phase flow inside tubes - convective boiling 9
3.4. 2-phase flow inside tubes - pressure drop 10
3.4.1. Other pressure drop effects 12

4. Experiment Setup **13**
4.1. CO_2 supply system - MARCO 13
4.2. The thermal mockup in HERA WEST 14
4.3. The thermal mockup in the test beam laboratories 16

5. Experimental Results **17**

6. Numerical Methods **19**
6.1. The programme 19
6.2. Computation of the parameters 21
6.2.1. Enthalpy 21
6.2.2. Pressure 22

7. Simulations **22**
7.1. Simulations performed 23

8. Conclusion **31**

A. Appendix **33**
A.1. Unit conversions 33
A.2. Additional simulations 34

1. Introduction

The Belle II experiment will be the upgrade of the Belle experiment. The Belle experiment collected a total integrated luminosity of 1000 fb^{-1} at the asymmetric positron electron collider KEKB in Tsukuba, Japan.
The collider will be upgraded to the SuperKEKB collider increasing its peak luminosity from $2.11 \cdot 10^{34} cm^{-2} s^{-1}$ to $80 \cdot 10^{34} cm^{-2} s^{-1}$ [1]. Therefore all detector components including the cooling system have to be redesigned.
A two-phase CO_2 cooling system will be used to cool the innermost detectors. It is superior to single-phase cooling because it is using a phase transition in addition to the convective cooling mechanism. Thus the two-phase cooling system has a higher cooling power per mass efficiency. Additionally by using CO_2 instead of fluorocarbons like C_3F_8, tube diameters can be reduced [2]. The number of radiation lengths seen by a particle passing through the detector are decreased and the accuracy of the detectors precision is increased. CO_2 also has the advantage that it is cheap and damage done to the environment by leaking gas or liquid is relatively small.
In the context of this thesis a two phase CO_2 cooling system for the Belle II experiment was analysed using computer based numerical finite element methods in MATLAB. A comparison with measured data was drawn. The objective of this thesis was to create dry out and pressure drop simulations of the inner detector cooling system of the Belle II spectrometer to gain a better understanding of the physics in the cooling system in order to maintain a safe operation of detectors in future.

The first chapter describes the Belle II experiment and the design of its upgraded spectrometer. In the second chapter, the experimental setup that was used to mimic the thermal conditions of the innermost detectors is explained. This is followed by a chapter presenting the theory needed for simulations. The next two chapters explain the experimental setups that were used to gain data and analyse them.
Subsequently the simulations are explained. In the last chapter a comparison between simulated and measured data is made, problems are discussed and conclusions drawn.

2. The Belle II Experiment

The Belle II Experiment is the upgrade of the Belle Experiment at KEK in Tsukuba Japan. The start of the operation is scheduled for the end of 2016. During the update of the KEKB collider to the SuperKEKB collider the luminosity is increased by a factor of 40. The current is increased by a factor of two and the beam size is reduced, while the beam-beam parameter is kept at KEKB value. The collision angle is increased from 22 mrad to 83 mrad and the asymmetry of the beam is shifted to 7 GeV (e^-) and 4 GeV (e^+) from 8 GeV (e^-) and 3.5 GeV (e^+). All these modifications increase the background levels by a factor of 10-20. For that reason a complete redesign of all detector components is necessary, including their cooling system.

2.1. The spectrometer

The spectrometer is displayed in Figure 1. The upper part shows the spectrometer as it is set up in Belle II, whilst the lower part of the figure shows its setup in the Belle Experiment.

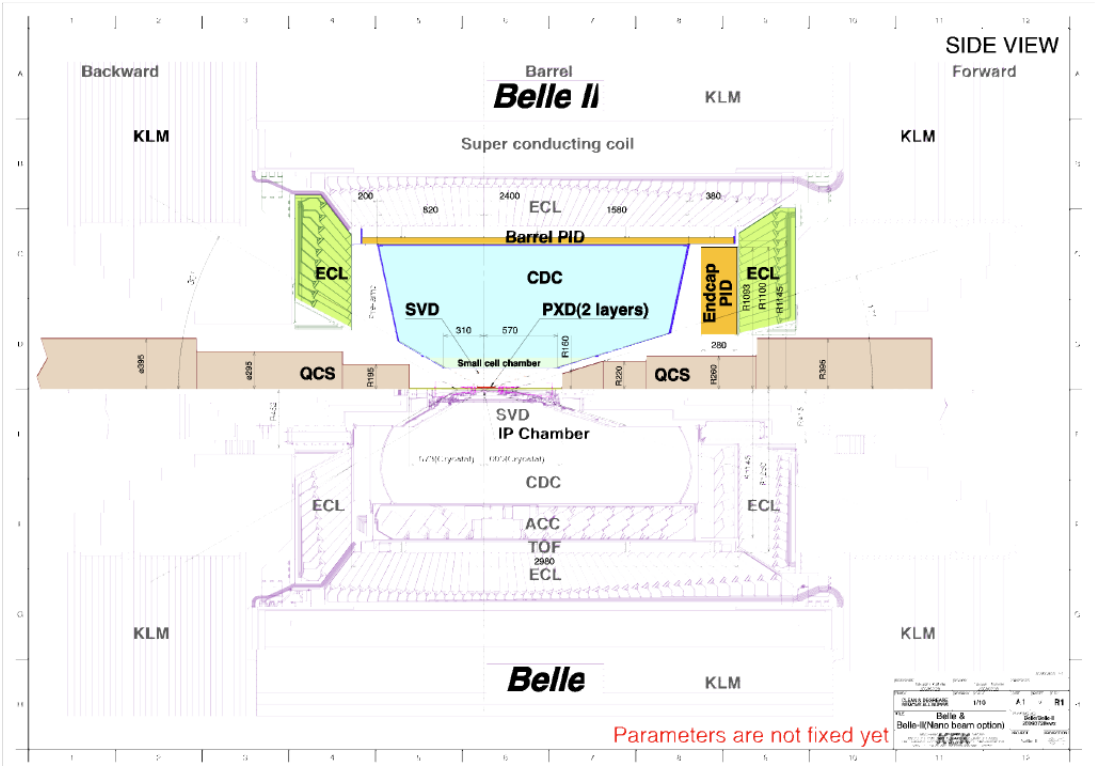

Figure 1: The Belle/Belle II spectrometers in comparison. The top of the diagramme shows the upgraded spectrometer. The bottom of the diagramme shows the old Belle spectrometer [1].

The spectrometer has an onion-like structure of subdetectors. The innermost spec-

trometer is composed of two layers of pixelated silicon sensors (PXD) and four layers of double-sided silicon strip sensors (SVD). These are embedded in a central drift chamber (CDC) followed by a barrel calorimeter (Barrel PID) and an electromagnetic calorimeter (ECL) placed inside a superconducting solenoid coil that provides a magnetic filed of 1.5 T. The outer shell is a K-long/Muon Detector (KLM). The cooling system analysed in this assignment will provide the thermal management for the PXD and SVD. PXD and SVD will be operated in a cold dry volume in which the temperature is kept above the dew point [11].

2.1.1. The Pixel Detector - PXD

Two layers of sensors will be placed as close as possible to the beam pipe. The PXD as it is mounted is displayed in Figure 2.

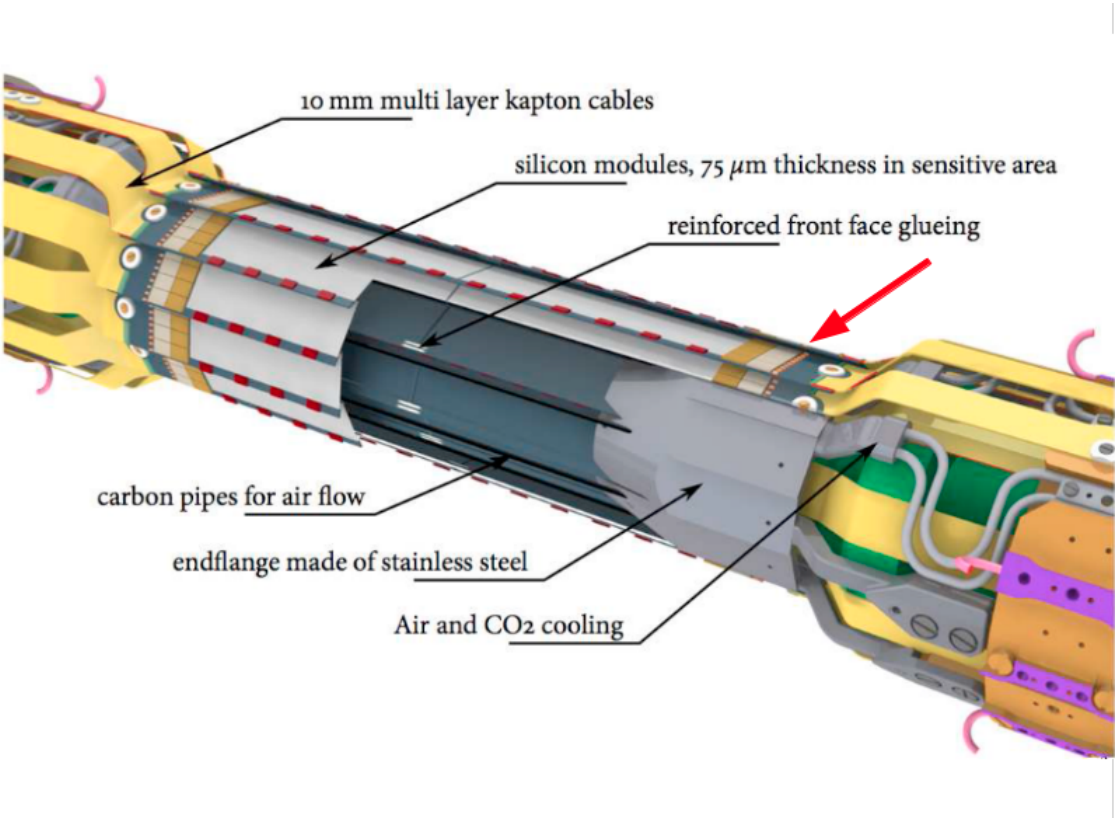

Figure 2: Installation of the PXD. The red arrow indicates the read out electronics. The SCB is the structure in grey [10].

The total thermal power of the PXD will be 360 W, 18 W being produced by each module. 16 W are dissipated by the readout chips that are placed at the ends of the module, 1 W by the detector chip itself and another 1 W by the switcher chips.
To prevent electromigration in the chips, they may not exceed a temperature above 30°C. The silicon sensors have to be kept at a temperature below 60°C. This is believed

to be made sure using a coolant temperature of -20° C. The cooling of the chips will be provided by the supporting structure, which acts as a heat sink. The cooling of the detector chips will be achieved by a moderate flow of N_2 at approximately -5°C and a speed of 1 m/s.

2.1.2. The Support and Cooling Block - SCB

The SCB will be used as a support structure of the PXD. It will also provide a heat sink to dissipate the thermal waste of the PXD's readout electronics. Additionally, the SCB is the injection nozzle for the N_2 flow that cools the PXD sensors. The PXD modules are mounted directly on the SCB. The PXD is composed of four SCBs, two for the top hemisphere and two for the bottom hemisphere respectively. 20 modules of silicon detector ladders are mounted on the SCB. A model of the design can be found in Figure 3.

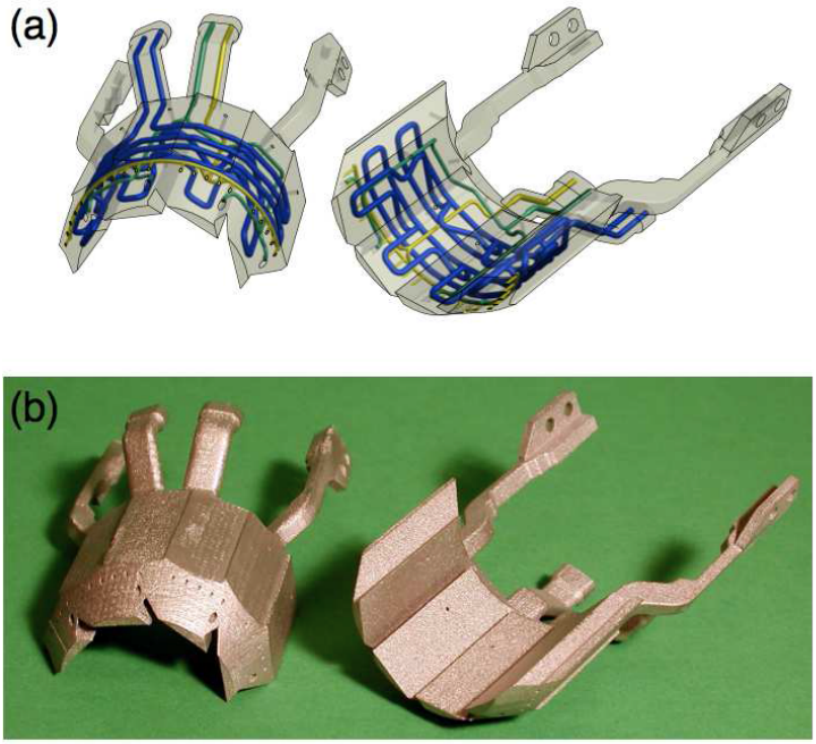

Figure 3: a) The design of the SCB. The blue line indicates the CO_2 channel. The green and yellow channel are used for the N_2 injection. b) SCB prototype [10].

The SCB modules are crafted from stainless steel using 3d-printers. The CO_2 channel is densely folded to maximise the area cooling the SCB's mass.

2.1.3. The Silicon Vertex Detector - SVD

The SVD consists of four layers of sensors that are mounted on endrings (Figure 4). The SVD has two hemispheres, similar to the PXD, built cylindrically around the beam pipe. The outer layers extend in length to cover as much angular space as possible. This is illustrated in Figure 5.

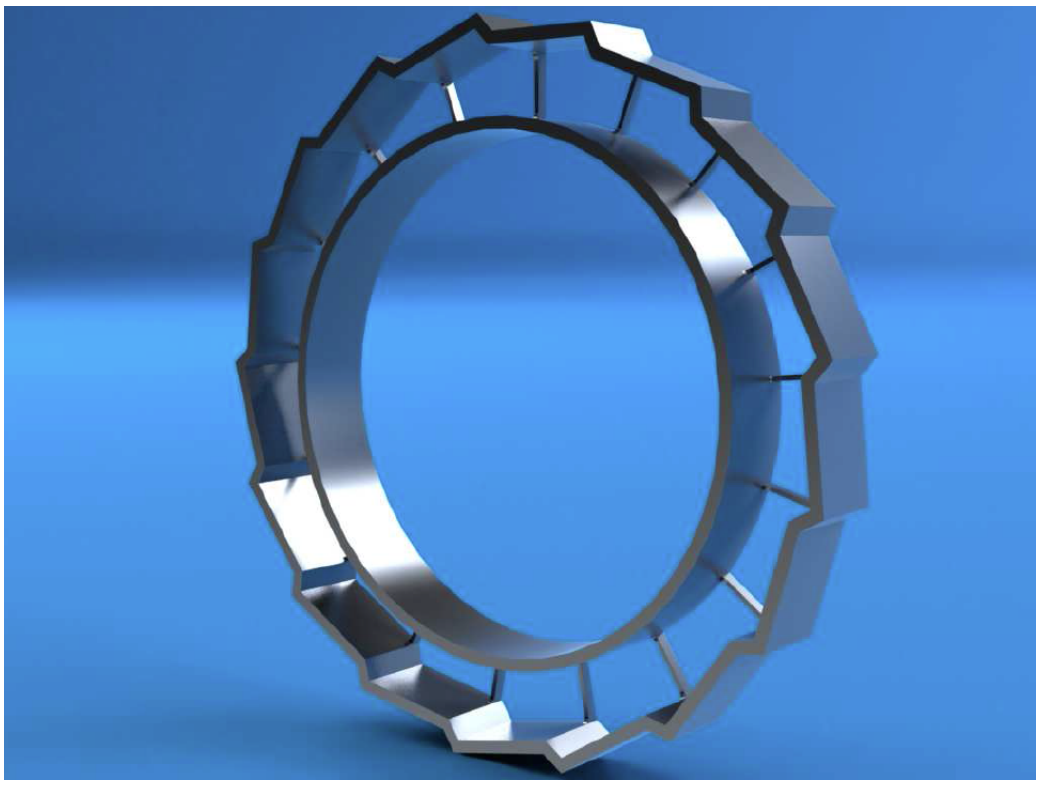

Figure 4: The endring design on which the sensor strips will be mounted. The endring is split into two components and the alignment tabs are not yet installed [1].

The cooling of the SVD will be done by clipping the cooling channels directly to critical places on most of the sensors. Some sensors will be cooled directly by the endrings. The main source of heat dissipation are the readout electronics (APV25 chips). There are 1902 chips installed in the SVD causing 0.35 W heat dissipation each, resulting in a total heat load of 665.7 W. The heat dissipation caused by the sensors will be taken up by the N_2 pumped into the dry volume.

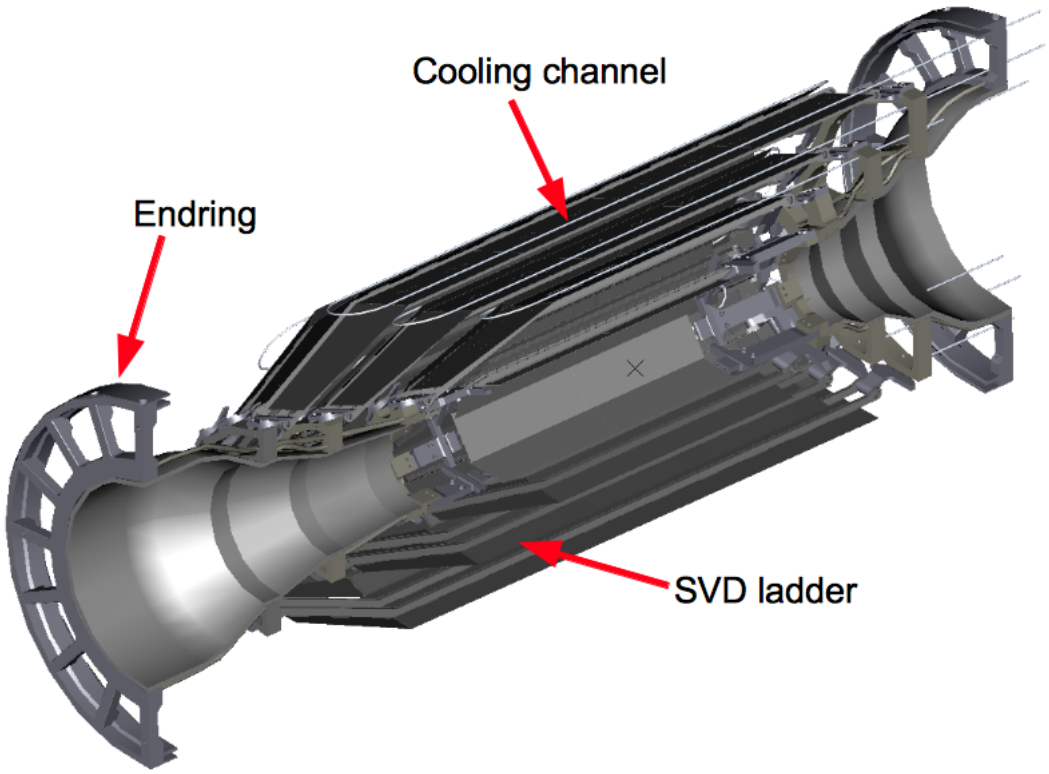

Figure 5: SVD split in half. The SVD ladders are mounted on half split endrings. Each layer-level has its own cooling channel [16].

3. Theory

This chapter presents and discusses the theory required to perform the simulations and to understand the experiments. The parameters used in the equations can be found in the Appendix, Table 4.

3.1. The 2-Phase State

Gibbs' Phase Rule states that in thermodynamic equilibrium the number of possible phases, P, a system can occupy is found from:

$$p = c + 2 - f$$

Where C is the number of chemical compounds in the system and f is the number of free parameters the system has. And that the minimum number of phase occupied in a system composed of one chemical ($c = 1$) is $p = 3$ when $f = 0$. Since $f = 0$ this can only be the case at one point - the Triple point.
Consequently the number of free parameters in a system is found from:

$$f = c - p + 2$$

In the in case where $p = 2 \rightarrow f = 1$. This shows that a 2-phase system still has one degree of freedom.

Thermodynamic equilibrium in can only exist as long as the change of the integrated free enthalpy $\Delta G = 0$, defined as:

$$G = U - S \cdot T + P \cdot V$$

and:

$$dG = -S \cdot dT + V \cdot dP \tag{3.1}$$

Where U is the internal energy, S is the entropy, T the temperature, V the occupied volume and P the pressure. So the parameters affecting the equilibrium are the change in pressure and in temperature. Therefore the 2-phase state can exist at a fixed pressure within a certain temperature range as well as at a fixed temperature within a certain pressure range.
The boundary of the range is the equality of the chemical potential μ_i of both phases. So $\mu_{\text{liquid}} = \mu_{\text{vapour}}$ has to hold. In reality this results in a 2-phase parabola below the critical temperature in the P-H-diagram - see Figure 6. Hence $H = U + P \cdot V$, equivalent to a P-V-diagram. The structure of this parabola and the critical values can be obtained by solving the Van-der-Waals or Dieterici equation of state. The critical temperature marks the root of the parabola. The position of the system on the isobar in the parabola is described by the vapour quality $x \in [0, ..., 1]$ where a vapour quality of zero describes a pure liquid with 0 amount of vapour, on the left of the parabola. A vapour quality of 1 resembles a pure gas on the right of the parabola.

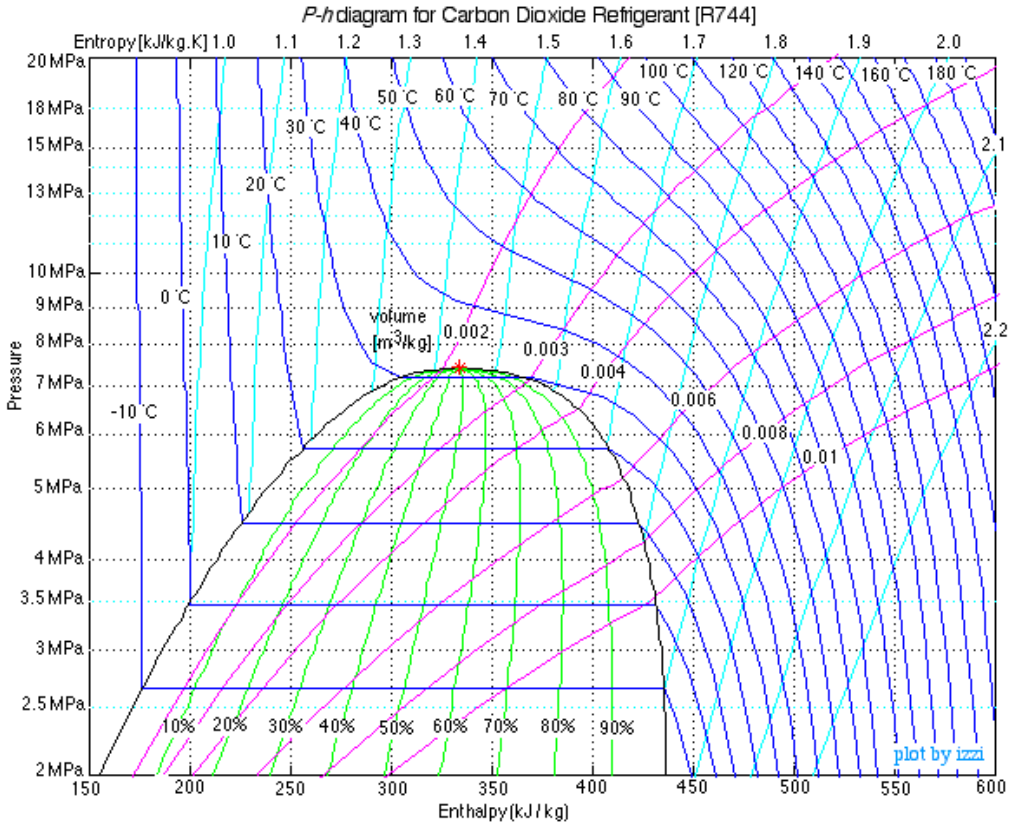

Figure 6: P-H-diagram of CO_2. The critical temperature of CO_2 is 30.978 °C and the critical pressure 73.77 bar [8]. The dark blue line represents the pressure in [MPa], the light blue line resembles the volume in [m^3/kg], the green line shows the vapour quality in percentage and the magenta coloured line displays the entropy in [kJ/(kg K)]. The top of the 2-phase dome is marked by a red star.

Note that the isotherm in the 2-phase parabola is parallel to the isovolumetric. This is due to the integral:

$$P(V_{\text{gas}} - V_{\text{liquid}}) = \int_{\Omega} P \cdot dV$$

being independent of the path Ω in the 2-phase parabola. And Equation 3.1 suggests $dG = 0 \rightarrow dP = 0 \Leftrightarrow dT = 0$.

3.2. Boiling

There are two modes of boiling inside tubes, nucleate boiling and film boiling. The one that occurs depends on the heat flux. Nucleate boiling results from a low heat flux. Small vapour bubbles form on nucleation sites at the surface - Figure 7a. In film boiling mode, the entire surface is covered in vapour - Figure 7b. This can only happen in heat fluxes above the critical heat flux. This is called dry out. The heat flux in the configurations to be tested will be below the critical heat flux. This concept applies to pools, when working in tubes, as in the case of this assignment, dry out can also be caused by turbulence.

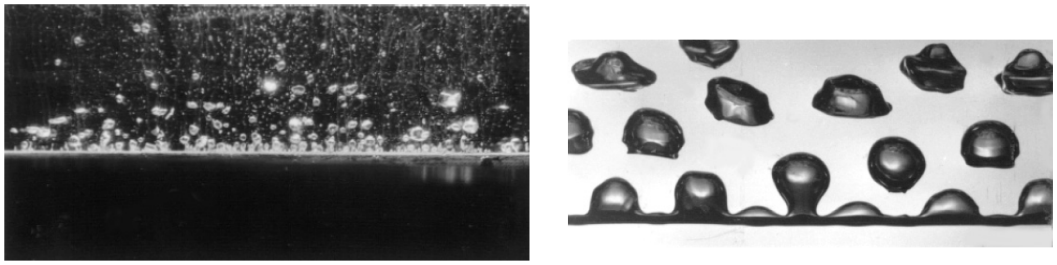

(a) (b)

Figure 7: a) Nucleate boiling: bubbles of vapour form on nucleation sites. b) Film boiling: the whole surface is covered in vapour. [12]

3.3. 2-phase flow inside tubes - convective boiling

Two models are presented to describe forced convection boiling inside tubes. One from L. Friedel [6] and one from J. G. Thome [4] and [5]. They are both based on the following theories. The boiling mechanism in a tube is a mixture of pure nucleate boiling and film boiling because of turbulence in the flow. Additionally, when the vapour quality rises, the amount of liquid decreases and film boiling becomes more evident in the tube, without critical heat flux having been applied to the tube. With a rising vapour quality different effects arise. In the Thome Model, these are accounted for by dividing the 2-phase regime into several flow patterns, each with a distinct function. The defined functions are used to calculate pressure drop and heat flux. The different flow regimes are displayed in Figure 8. The Friedel Model treats the 2-phase state as a homogenous mixture, described by a 2-phase multiplier.

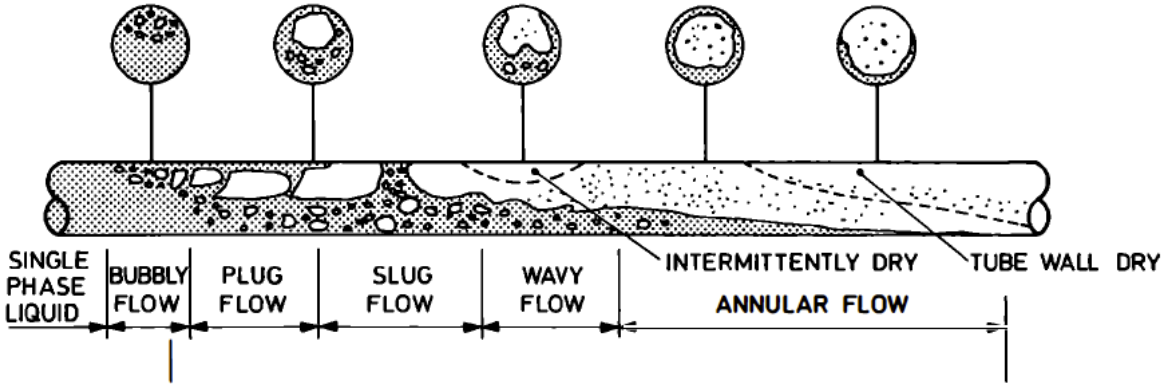

Figure 8: Different flow regimes in convective flow boiling inside tubes [12].

In general, the heat flux through tube walls can be derived from Fourier's law:

$$\dot{Q}_{\text{env}} = \frac{\Delta T}{\frac{1}{\alpha_{\text{i}} A_{\text{i}}} + \frac{1}{\alpha_{\text{o}} A_{\text{o}}} + \frac{1}{2\pi \cdot L \cdot \lambda_{\text{tube}}} \ln\left(\frac{d_{\text{o}}}{d_{\text{i}}}\right)} \tag{3.2}$$

Where $A_{\text{i/o}}$ is the inner/outer surface of the tube, $d_{\text{i/o}}$ is the inner/outer tube diameter, L the length of the tube, λ the thermal resistance of the tube and $\alpha_{\text{i/o}}$ the inner/outer heat transfer coefficient. This coefficient is constant for air external to the tube but has to be dynamically calculated for liquid inside the tube. The critical variable for the purpose of this discussion is α_i, the heat transmission coefficient of the fluid inside the tube.
Applying the Thome Model, the heat transmission coefficient α_{i} is derived from:

$$\alpha_{\text{i}} = \frac{\theta_{\text{dry}} \alpha_{\text{V}} + (2\pi - \theta_{\text{dry}}) \alpha_{\text{wet}}}{2\pi}$$

The transmission coefficient is a function of the individual state. The dry out angle θ_{dry}, the liquid heat transfer coefficient α_{wet} and the vapour heat transfer coefficient α_{V} are functions of this individual state. It is important to note that for all states where the tube wall is wet, the heat transmission coefficient has the same order of magnitude. As soon as the the tube wall dries out the heat transmission coefficient drops by several orders of magnitude. For exact calculation methods please see [5].
Using the Friedel Model the heat transfer coefficient is calculated via the Dittus-Boelter equation ([15]):

$$\alpha_{\text{i}} = \frac{\lambda}{d_{\text{i}}} \left(0.023 \cdot Re^{0.8} \cdot Pr^{0.4}\right).$$

3.4. 2-phase flow inside tubes - pressure drop

In general, pressure drop is composed of three parts momentum, gravity and friction. giving:

$$\Delta P = \Delta p_{\text{m}} + \Delta p_{\text{g}} + \Delta p_{\text{f}} \tag{3.3}$$

The pressure drops from momentum and gravity are calculated using a similar approach. In order to calculate momentum, a separate flow model is used which is sensitive to the relative fraction of liquid and vapour flowing inside the tube.

$$\Delta p_{\mathrm{m}} = \dot{m}^2 \left\{ \left[\frac{(1-x)^2}{\rho_{\mathrm{L}}(1-\varepsilon)} + \frac{x^2}{\rho_{\mathrm{V}}\varepsilon} \right]_{\mathrm{out}} - \left[\frac{(1-x)^2}{\rho_{\mathrm{L}}(1-\varepsilon)} + \frac{x^2}{\rho_{\mathrm{V}}\varepsilon} \right]_{\mathrm{in}} \right\}$$

The pressure drop is mainly dependent on mass flow, $\dot{m}$ and the vapour quality, x. The other components in the equation are defined in the Unit Conversion Table in the Appendix.

The gravitational pressure drop is derived from a homogenous flow model :

$$\Delta P_{\mathrm{g}} = g \cdot \rho_{\mathrm{H}} \cdot \Delta h \cdot sin(\theta)$$

The gravitational pressure drop is mainly influenced by the change in height, Δh. The homogenous density, ρ_{H}, and its dependent variables can be found in [4].
The frictional pressure drop can be calculated using two different approaches. Depending on either the Thome Model or the Friedel Model. The Thome model uses flow patterns for each individual state. For example, the frictional pressure drop for the liquid phase is found by:

$$\Delta P_{\mathrm{liq}} = 4 f_{\mathrm{liq}} \frac{L}{d_{\mathrm{eq}}} \frac{\dot{m}}{2 \cdot \rho_{\mathrm{L}}}$$

To give another example, the frictional pressure drop flow pattern for stratified wavy flow is calculated from:

$$\Delta P_{SW} = 4 f_{\mathrm{SW}} \frac{L}{d_{\mathrm{eq}}} \frac{\rho_{\mathrm{V}} \cdot u_{\mathrm{V}}^2}{2}$$

The Friedel Model uses a different approach to calculate the frictional pressure drop using a dimensionless 2-phase multiplier ϕ to account for the 2-phase behaviour:

$$\Delta P_{\mathrm{f}} = \phi^2 \cdot \Delta P_{\mathrm{liq}}.$$

The Two phase multiplier $\phi^2 > 1$ is derived from Friedel's correlation. For more details see [6]. The liquid pressure drop is arrived at through the Darcy-Weißbach equation:

$$\Delta P_{\mathrm{liq}} = f_{\mathrm{D}} \frac{L}{d_{\mathrm{eq}}} \frac{\rho_{\mathrm{L}}}{2} u_{\mathrm{L}}^2$$

Where the friction factor f_{D} is found from either by solving the Coolebrock equation for turbulent flow:

$$\frac{1}{\sqrt{f_{\mathrm{D}}}} = -2 \cdot \log_{10} \left(\frac{\varepsilon}{3.7 \cdot d_{\mathrm{eq}}} + \frac{2.51}{Re \cdot \sqrt{f_D}} \right)$$

or the Blasius equation for laminar flow:

$$f_{\mathrm{B}} = \frac{0.184}{Re^{0.2}}$$

If the Reynolds Number, Re, is above 4 000, the Coolebrock equation is used. If Re is below 4 000 the Blasius equation is taken. In the case Re being smaller than 2 300, the Blasius equation simplifies to:

$$f_{\mathrm{B}} = \frac{64}{Re}.$$

Note that the Reynolds Number is a function of the mass flow:

$$Re = \frac{\dot{m} \cdot d_{\mathrm{eq}}}{v}$$

3.4.1. Other pressure drop effects

The previously discussed pressure drop effects are only applicable to straight tubes of constant diameter. More complex geometries such as bent tubes, or tubes of different diameter stuck together, are discussed below.
The calculation for a bent tubes is modelled on a longer tube with an equivalent pressure drop. In the case of 2-phase flow, a 2-phase multiplier is multiplied by the computed pressure drop. The single-phase liquid phase pressure drop for bent tubes is derived by:

$$\Delta P_{\mathrm{bend}} = \frac{\zeta}{2\rho_{\mathrm{L}}} \cdot \frac{L}{d_{\mathrm{eq}}} \left(\frac{\dot{m}}{\frac{\pi}{4} \cdot d_{\mathrm{eq}}^2} \right) \tag{3.4}$$

$\zeta \in [0, ..., 1]$ is a dimensionless scalar.
In a 2-phase scenario, the pressure drop is derived in the same way as through the Friedel model:

$$\Delta P_{\mathrm{bend\ two\ phase}} = \phi^2 \cdot \Delta P_{\mathrm{bend}} \tag{3.5}$$

In the case of cross-section reductions, there are two types to consider: decreasing and increasing cross-sections.
To calculate decreasing cross-sections one has to use the formula:

$$\Delta P_{\mathrm{c-s-change}} = \zeta_{\mathrm{E}} \frac{\rho_{\mathrm{L}} \cdot u_{\mathrm{L}}^2}{2} \tag{3.6}$$

Here $\zeta_{\mathrm{E}} \approx a - 0.4 \cdot f_2/f_1$ and $a \approx 0.425$, and $f_1 > f_2$ represent the cross-sections of the tubes. This is only valid for turbulent flow where $Re \to \infty$. For laminar flow, an offset off $a \approx 1.05$ has to be chosen.
For increasing cross-sections one uses:

$$\Delta P_{\mathrm{c-s-change}} = \left(1 - \frac{f_1}{f_2}\right)^2 \frac{\rho_{\mathrm{L}} \cdot u_{\mathrm{L}}^2}{2} \tag{3.7}$$

A tube distributor can be modelled as serially connected t-pieces and one standard branch. The pressure drop of the t-pieces is calculated by averaging the pressure drop across all t-pieces. This extrapolation is possible as they are connected in a series. In this case the pressure drop over the parallel tubes must to be equal. The pressure drop across a single t-pieces is calculated using Equation 3.6, where $\zeta = 0.85$ for lines exiting

the distributor and $\zeta = 0.25$ for lines entering the distributor.
The pressure drop across valves is calculated in the same way, where ζ_{valve} ranges from 3 to 5 [13].

4. Experiment Setup

Two experiments to mimic the circumstances as they will appear in the detector operation in Belle II were set up. One was set up in a laboratory in the HERA WEST hall at DESY in Hamburg. This experiment was conducted to study the cooling power of the SCBs and to get familiar with the operation of MARCO. The other experiment was set up in the Test Beam Facility at the Synchrotron 2 at DESY. This experiment was set up to provide the cooling for the future test beam experiments. The data gained from the first test runs could be used in the context of this assignment.
The setup of the experiments is explained in this chapter.
The experiments can be considered in two parts - the thermal mockup and the CO_2 supply system.

4.1. CO_2 supply system - MARCO

A Multipurpose Apparatus for Research on CO_2 (MARCO) is used as the CO_2 source for the experiment. MARCO uses a 2-phase accumulator controlled loop to provide CO_2 of a set point temperature [2]. An overview of the apparatus can be found in Figure 9.
Two pumps - PM101 and PM102 in Figure 10 - provide the mass flow to the experiment. The adjustable mass flow ranges from 5 g/s to 30 g/s. A pressure drop above 10 bar triggers a security algorithm shutting down the pumps. This results in an upper limit of approximately 12 g/s depending on the experiment connected. The pressure drop is measured between the outgoing (PR106 in 10) and incoming (PR118 in 10) CO_2 flows. The CO_2 is cooled by a chiller (HX101 in 10). The temperature of the cooled liquid can be set between 25° and -40°. The pressure controlled by heating or cooling the accumulator.
MARCO can be completely controlled via computer, and all parameters set and read from there.

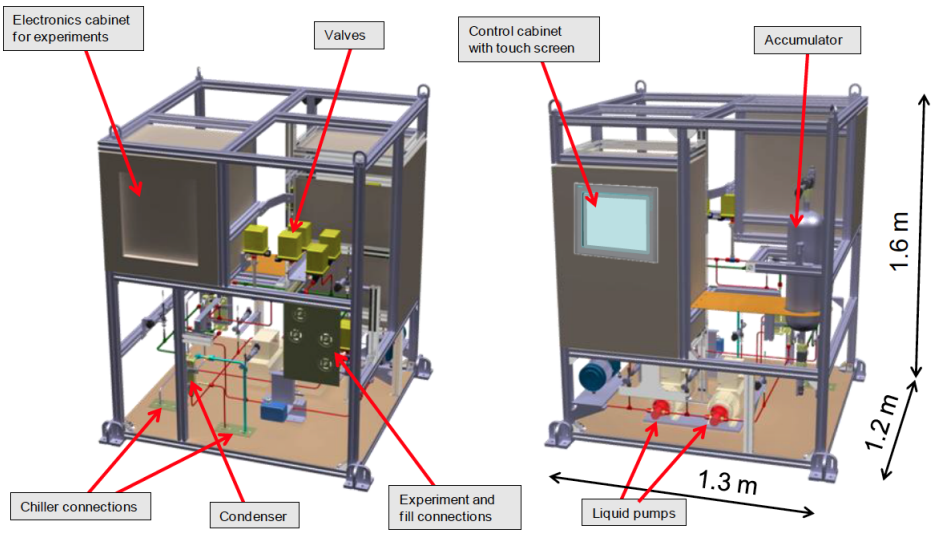

Figure 9: Overview of MARCO [9].

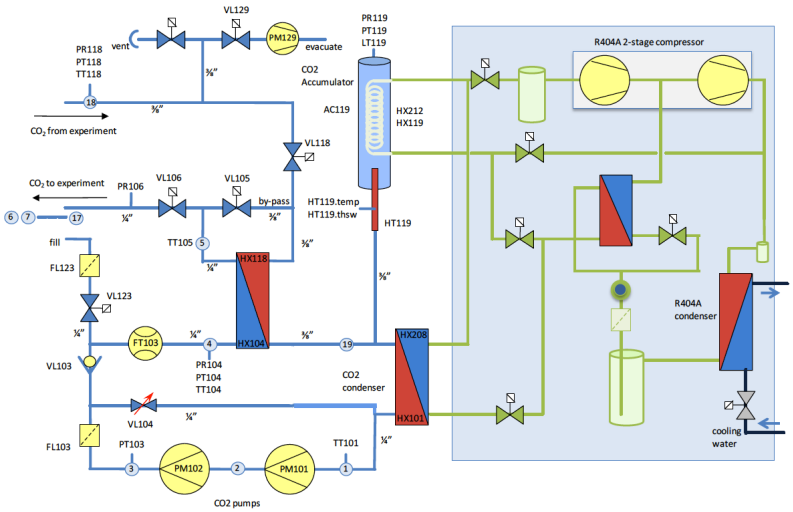

Figure 10: Design layout of MARCO. The blue highlighted part is the chiller. The CO_2 is cooled by the chiller. The pressure can be controlled by an accumulator (AC119). The mass flow of the CO_2 is driven by 2 pumps (PM101 and PM102) [9].

4.2. The thermal mockup in HERA WEST

The thermal mockup in the HERA WEST setup consists of the support and cooling block (SCB) and its supplying tubes. There are four parallel SCBs and a heater fed by a distributor which is connected to MARCO. The transfer lines connecting the distributor

and the SCB inlets are isolated against the environment by a vacuum of approximately $1 \cdot 10^{-5}$ bar.
The tube from MARCO to the distributor is 3.27 m in length. The distributor is 0.9 m long the return tubes have the same parameters. One branch of SCB line consists of 8 m of vacuum isolated transfer line, consisting of three cooper tubes, a 0.12 m outlet, SCB inlets of 0.12 m and, 0.5 m the SCB itself. The return line to the distributor is similarly arranged. A more detailed description can be found in Table 2 and Figure 17. The length of the tubes connecting the distributor and the SCB-inlets is chosen such that the fluid will be saturated by pressure drop as it enters the SCB.

On the SCBs there are thermal MHP-20 resistors glued onto a copper plate to simulate the heat load dissipated by the PXD. Each SCB has a heat probe glued on one of the copper plates to monitor the temperature. A temperature higher than 60°C would trigger a safety loop and shut down the power supply to the heaters on the SCBs. A picture of the setup is shown in Figure 12.
Another heater runs parallel to the SCB lines, and consists of a 0.86 m long concentric tube with a heater element as its core. This construction will be used to mimic SVD behaviour in later studies.

MARCO is a 2-phase accumulator controlled loop circle (2-PACL) device delivering the flow of cooled CO_2. Data is acquired though MARCO's interface. Figure 11 depicts the setup.

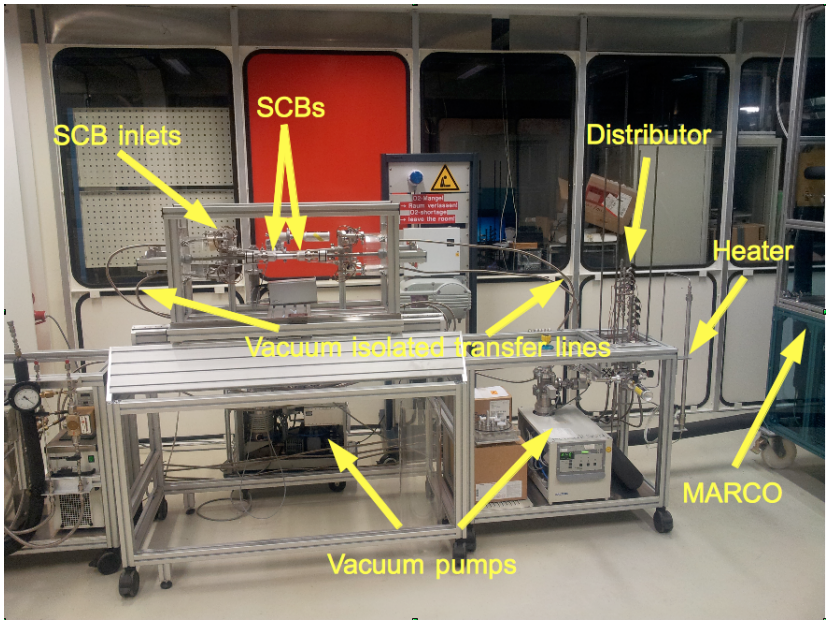

Figure 11: The HERA WEST set up. The thermal mockup of the PXD is in the centre of the photograph. MARCO is in the right hand corner.

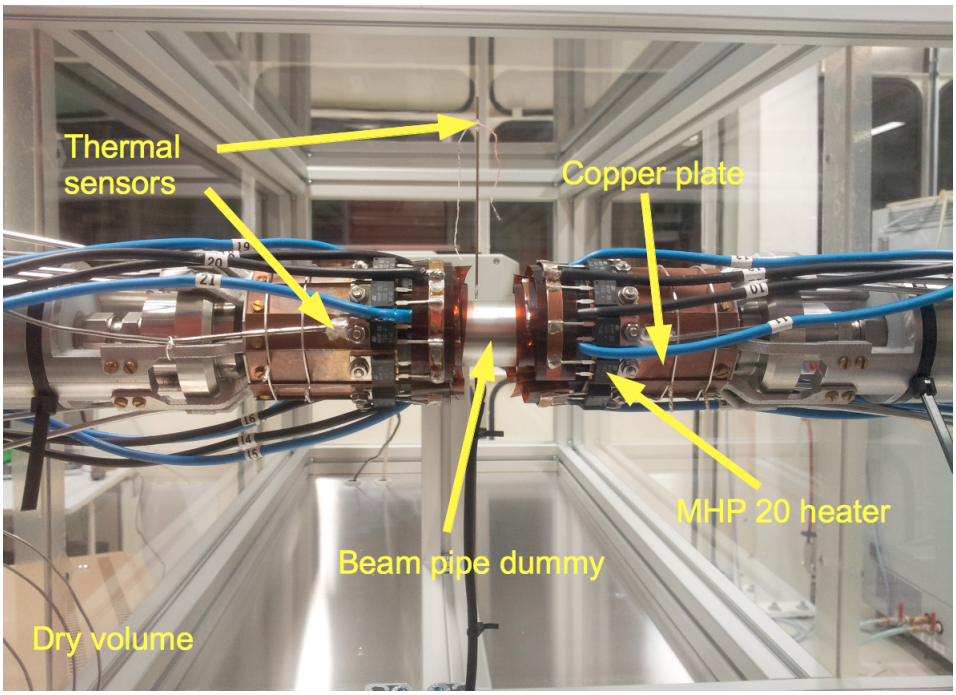

Figure 12: Close-up view of the SCBs in the thermal mockup. In a dry volume with heaters mounted on copper plates screwed to the top of the SCBs.

4.3. The thermal mockup in the test beam laboratories

The thermal mockup in the test beam laboratories is organised similarly to the HERA WEST setup. Despite there being six parallel lines fed by the distributor, only 4 were used. A heater was installed in series in the returning line to MARCO. There is no SCB connected between the transfer lines. The inner and outer tube of the concentric line are connected directly with each other. See Figure 13.
The distributor and MARCO were connected 3.9 m of tube, and 12.3 m of concentric transfer line provided a connection to and from the adjacent experimental area. The inner and outer part of the concentric line are connected with a 0.3 m tube extension using a t-piece.

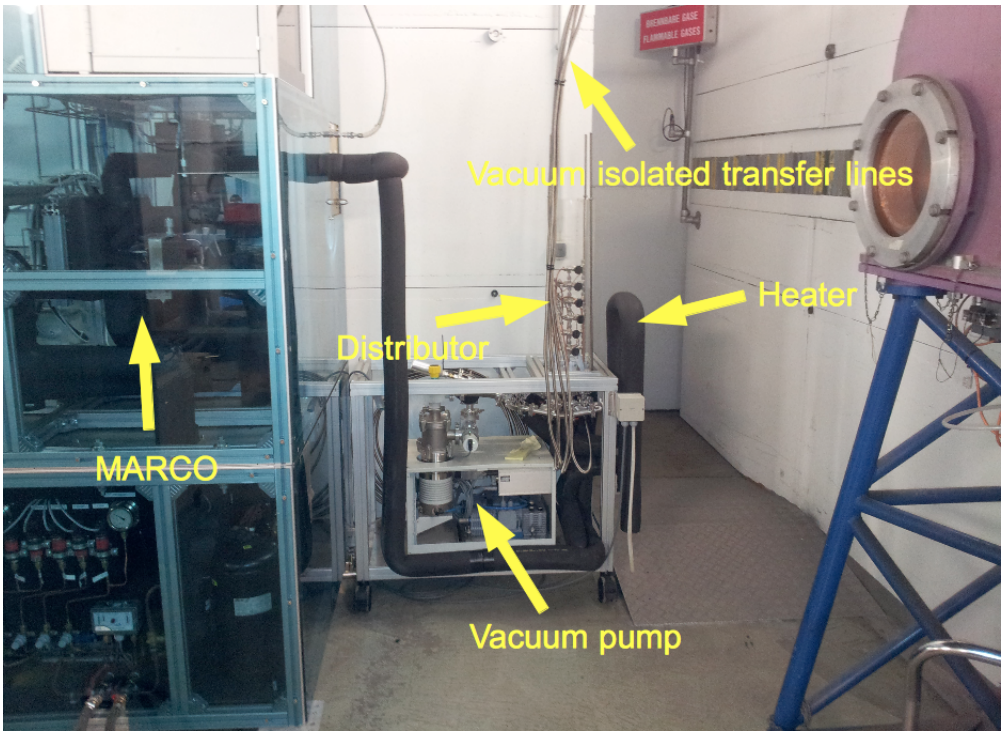

Figure 13: The test beam laboratory. MARCO is on the left of the photograph, the distributor is in the centre. The transfer lines go to the neighbouring laboratory.

5. Experimental Results

The HERA WEST setup was used to perform the experiments that provided the first three sets of measurements. MARCO was then moved to the test beam laboratories before proceeding with further experiments.

An initial measurement was conducted to investigated the pressure drop over two parallel SCBs to control if all SCB were manufactured equivalently. It was was not possible to measure a single SCB, because the pressure drop was above 10 bar and the security loop would have shut down MARCO. Thus two SCBs in parallel were taken. All possible combinations of the four SCBs were measured at a total mass flow of 5 g/s and with no heat load applied. The results can be found in Table 1.

No significant difference in the manufacturing quality of the SCBs was found. All discrepancies were within the range of the error margin. This enabled the pressure drop over the experiment to be interpreted as an average pressure drop over one of the PXD cooling lines in subsequent measurements. The total mass flow was divide by the number of lines supplied from the distributor.

In the next measurement only the pressure drop on the heater was measured. The supply lines to the distributor were all closed and no heat load was applied.

The results are displayed in Figure 14.

Table 1: Results of the equality measurement. The SCBs are numbered from 1 to 4. The numbers display the pressure drop over two SCBs in bar at a total mass flow of 5 g/s.

#	**#1**	**#2**	**#3**	**#4**
#1	x	4.3±0.2	4.1±0.2	4.1±0.2
#2	4.3±0.2	x	4.2±0.2	4.3±0.2
#3	4.1±0.2	4.2±0.2	x	4.1±0.2
#4	4.1±0.2	4.3±0.2	4.1±0.2	x

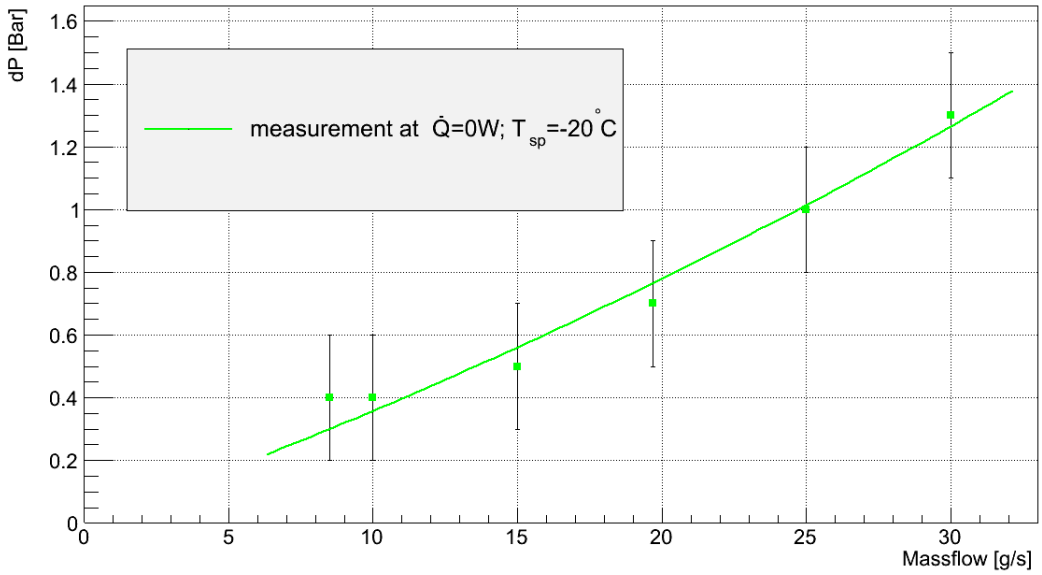

Figure 14: Measured pressure drop on heater only.

While performing this measurement the upper mass flow boundary was found to be 30 g/s. In addition is was possible to determine that the pressure drop from the non-linear part of the curve was smaller than the linear part. It could be that the gravitational effects are more evident than frictional, when comparing MARCO and the mockup. As the pressure drop characteristics of MARCO and the filters are unknown this explanation remains theory at this stage.
A further reading was taken to measure the pressure drop on all 4 SCBs related to the heat load applied. The results are depicted in Figure 15. To access lower ranges of mass flow in the heated measurements the heat source on one line was turned off. Using fit function from measurements taken under unheated conditions it was possible to determine the mass flow in the unheated branches by solving $dP = h(x)$ for x. The mass flow in the other branches then is consequently $\dot{m} = \dot{M} - n \cdot x$, where $\dot{M}$ is the total mass flow, x the mass flow found from the fit function, and n the number of unheated

branches. The fit function of the unheated measurement is:
$h(x) = 0.69 \pm 0.05 \cdot x + 0.43 \pm 0.02 \cdot x^2$
While this measurement was conducted the temperature on the heaters did not exceed $60° C$ and the safety loop was not triggered. A recording of the temperature of the sensors on the SCBs was not possible. It can not be concluded if a dry out in the SCB occurred because two SCBs were measured in parallel and a dry out at the end of a single one might not cause a measurable effect due to the high thermal conductivity of the modules.

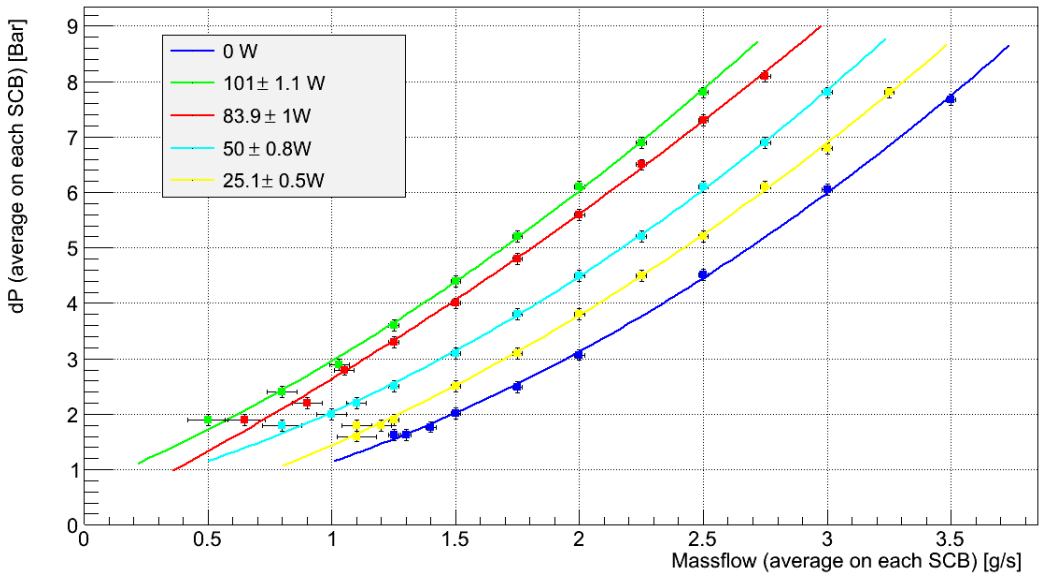

Figure 15: Measured pressure drop on parallel SCBs under equal conditions. The mass flow was determined by dividing the total mass flow by the number of parallel branches. The first three points of the heated measurements have been extrapolated using the fit function of the unheated measurement.

6. Numerical Methods

This chapter gives an overview of the numerical methods used in the simulations, and the structure of the programme CoBra.

6.1. The programme

The MATLAB function CoBra [3] was used to perform the simulations. The structure of this function is depicted in Figure 16. The function calculates the thermodynamical properties of one branch of PXD cooling line as it runs from the distributor through the experiment and back to the distributor. A finite element convergence mechanism is used to calculate pressure drop and heat transfer of CO_2 evaporation inside the tubes, based

on the Cheng-Ribatski-Wotjan-Thome CO_2 flow pattern map [4], [5] in MATLAB. The structure of the dependencies between the variables of this mechanism is displayed in Figure 16.

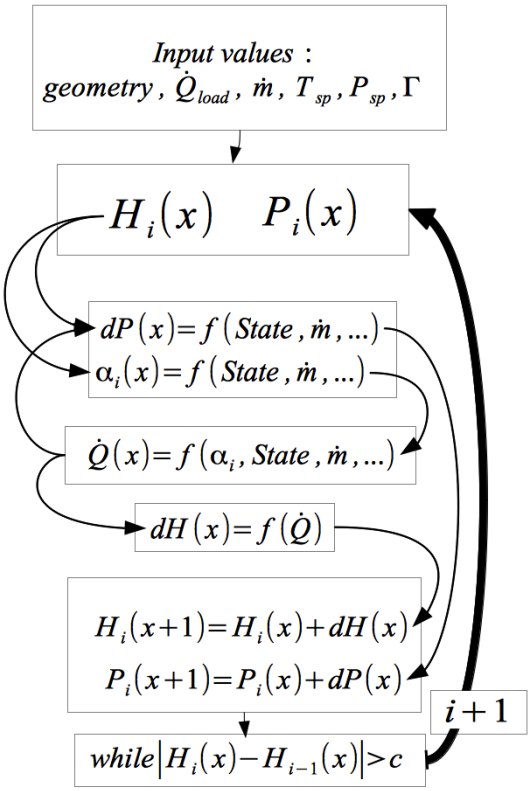

Figure 16: Structure of the CoBra subroutine Cooling Branch. The arrows indicate dependencies between the parameters.

A geometry file is called up by MATLAB and basic tube-dependent parameters, such as the length of the tubes etc. are assigned. The boundary condition is a fixed-outlet pressure, based on the temperature set point T_{sp}. This set point is calculated by the MATLAB subroutine refprop.m (NIST) that uses REFPROP (NIST).

The geometry is chopped into y sections where each section represents one tube as it was defined in the geometry file. These sections are again chopped into z smaller sections to represent the finite elements. The starting values $H_i(z)$ and $P_i(z)$ are calculated based

on a set point temperature T_{sp} defined by the user, where i is the number of the iteration and z is the number of the finite element.

The euclidian norm of the H-vector relative to its value in the previous iteration was chosen as convergence criterium of the while loop. Such that:

$$\sqrt{\sum_{z} (H_{\mathrm{i}}(z) - H_{\mathrm{i-1}}(z))^2} \;=\; |\vec{H}_{\mathrm{i}}(z) - \vec{H}_{\mathrm{i-1}}(z)| < c$$

Where c is a constant set to $0.01\,\mathrm{J/kg}$.
The enthalpy was chosen because it displays the heat uptake (δQ):

$$\begin{aligned} dH &= T \cdot dS + V \cdot dP \qquad\qquad |T \cdot dS = \delta Q \\ &= \delta Q \end{aligned}$$

Within an element the pressure drop was considered to be zero. The properties $H = f(P,T)$ and $P = f(T)$ were calculated using REFPROP. The parameters H_0 and P_0 used for the iteration start were calculated from the temperature set point.

6.2. Computation of the parameters

The following gives a more detailed description of how the parameters in Figure 16 were calculated.

6.2.1. Enthalpy

Enthalpy is a function of the heat load. The enthalpy defines the state (=flow pattern in the Thome Model) of a single finite element. The derivation of which is discussed here. The local enthalpy gradient dH is computed using:

$$dH = \frac{\dot{Q}}{\dot{m}}$$

So that the enthalpy of a single element can be computed by:

$$H(z+1) = H(z) + dH(z)$$

$\dot{Q}$ is calculated using the following relationship:

$$\dot{Q} = \dot{Q}_{\mathrm{load}} + \dot{Q}_{\mathrm{env}} + \dot{Q}_{\mathrm{ex}}$$

$\dot{Q}$ is the total heat flow. $\dot{Q}_{\mathrm{load}}$ is the heat flow from the applied heat load and $\dot{Q}_{\mathrm{env}}$ is the heat flow to the environment caused by the temperature gradient to the environment respectively. The environmental temperature T_{env} is set to $20^{\circ}\,C$.
One can find:

$$\dot{Q}_{\mathrm{load}} = \mathrm{const.}$$

Because the heat dissipation of the PXD readout electronics is considered to be constant, and the tube-tube exchange term:

$$\dot{Q}_{\mathrm{ex}} = 0$$

Which is the case for non concentric tubes. Using equation 3.2 one can find:

$$\dot{Q}_{\mathrm{env}} = \frac{T_{\mathrm{env}} - T(z)}{\frac{1}{\alpha_{\mathrm{i}}(z)A_{\mathrm{i}}(z)} + \frac{1}{\alpha_{\mathrm{o}}(z)A_{\mathrm{o}}(x)} + \frac{1}{2\pi\cdot(L(z+1)-L(z))}\underbrace{\left(\frac{1}{\lambda_{\mathrm{insu}}}\ln\left(\frac{d_{\mathrm{o}}+2d_{\mathrm{insu}}}{d_{\mathrm{o}}}\right) + \frac{1}{\lambda_{\mathrm{t}}}\ln\left(\frac{d_{\mathrm{o}}}{d_{\mathrm{i}}}\right)\right)}_{=\,\Gamma}}$$

$$= \frac{T_{\mathrm{env}} - T(z)}{\frac{1}{\alpha_{\mathrm{i}}(z)A_{\mathrm{i}}(z)} + \frac{1}{\alpha_{\mathrm{o}}(z)A_{\mathrm{o}}(z)} + \frac{1}{2\pi\cdot(L(z+1)-L(z))}\cdot\Gamma(z)}$$

Note that in contrast to Equation 3.2, this equation has an insulation term. The geometry factor Γ is already calculated in the geometry file as it only consist of external parameters. The geometry factor represents the thermal resistance of the tube and its insulation from the environment. Q_{load} ranges from 0 W to 100 W.

This programme could also be used to calculate concentric tubes, in which case Q_{ex} will be set to greater or less than zero using the equation:

$$\dot{Q}_{\mathrm{ex}} = \frac{T(z) - T(z')}{\frac{1}{\alpha_{\mathrm{i}}A_{\mathrm{i}}} + \frac{1}{\alpha_{\mathrm{o}}A_{\mathrm{o}}} + \underbrace{\frac{1}{\Delta L(z)}\left(\frac{1}{2\pi\lambda_{\mathrm{t}}}\ln\left(\frac{d_{\mathrm{o}}}{d_{\mathrm{i}}}\right)\right)}_{=\,\mathrm{R_t}}}$$

Where $\mathrm{R_{tube}}$ is the thermal resistance of the tube between the fluids. Since it is an external parameter it is also calculated in the geometry file.

6.2.2. Pressure

The pressure is calculated from initial pressure P_0 and the pressure drop dP:

$$P(z+1) = P(z) + dP(z)$$

Where z displays the number of the finite element. The pressure drop is determined from Equation 3.3. For the implementation of Equation 3.4, 3.6 and 3.7 a flag vector $flag(z)$ that is filled with zeros has been defined in CoBra. Only locations with bends or changes in diameters carry a number one. "If conditions" within the programme check if the functions for the equations have to be called upon.

7. Simulations

CoBra was used to simulate experiments. The measured pressure drop could not be reproduced in adequate accuracy by the simulation. This section analysis the problems

encountered, and identifies and discusses potential solutions.

7.1. Simulations performed

First the HERA WEST setup was simulated.
The temperature set point was set to -20° C. The geometry used is displayed in Table 2.
The Main pressure drop took place in tube 9 - the SCB.
Because the distributor supplied 4 parallel PXD branches, the mass flow has to be multiplied by a factor of 4 at the distributor inlets. The distributor inlets were the first and last 5 tubes in the geometry. Gravitational effects in the distributor (tube 5 & 13) were neglected.
Γ of tube 6 and 12 was set to zero. These were the transfer lines from the distributor to the SCB inlets and back. These lines had an isolating vacuum, so there was no temperature gradient to the environment.

Table 2: MARCO geometry: as this geometry was used, the mass flux $\dot{m}$ as multiplied by 4 on the first and last 5 tubes. This had to be done because the distributor supplied 4 parallel PXD branches. See Figure 17 for a sketch of this geometry.

#	d_i **[mm]**	**L [m]**	θ **[°]**	Γ **[W/(K·m)]**
#1	6	0.17	0	0.1
#2	6	1.4	90	0.1
#3	6	1.4	0	0.1
#4	6	0.3	-90	0.1
#5	6	0.9	0	0.1
#6	2	8	0	0
#7	2	0.12	0	0.62
#8	1.7	0.12	0	0.57
#9	1.2	0.5	0	0.50
#10	1.7	0.12	0	0.57
#11	2	0.12	0	0.62
#12	2	8	0	0
#13	6	0.9	0	0.1
#14	6	0.3	90	0.1
#15	6	1.4	0	0.1
#16	6	1.4	-90	0.1
#17	6	0.17	0	0.1

The models are not able to describe measured pressure drop sufficiently. The correlation of applied heat load and pressure drop can not be projected correctly. They fail to predict the observations without heat load by at least a factor of 3 if the function is not altered to fit the geometry - see Figure 26 and Figure 27 in the Appendix.

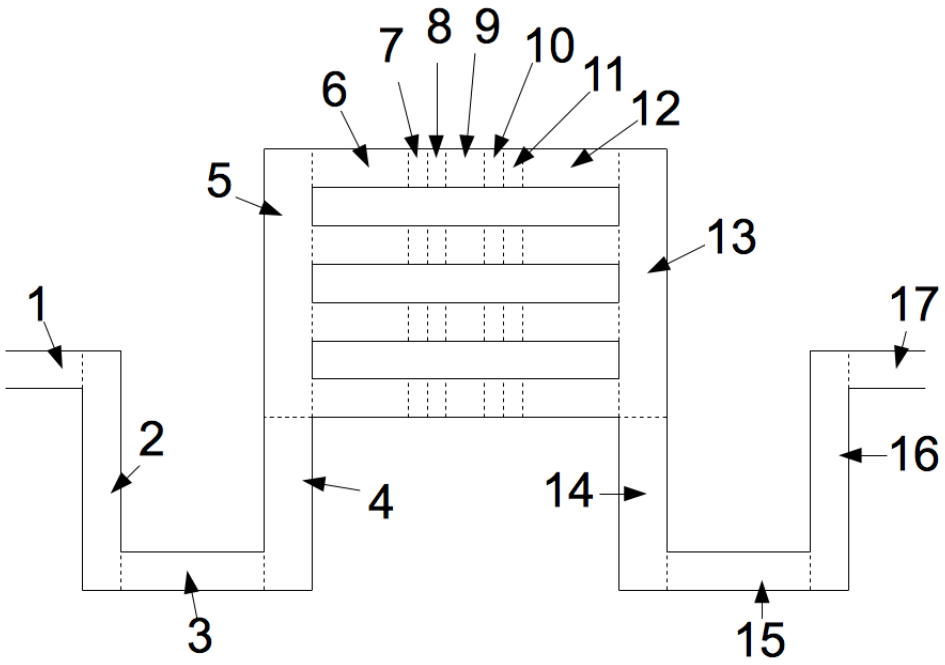

Figure 17: Sketch of the geometry in the HERA WEST setup not to scale. See Table 2 for the parameters of the tubes. Tubes 1 and 17 are connected to MARCO.

In subsequent simulations, the Friedel Model was used, because it initially gave better results. Additional simulations using the Thome Model can be found in the Appendix. The first alteration to the simulation was the introduction of bends to introduce more friction in the SCBs, as the densely folded channel in the SCB was thought to be the main cause for pressure drop in the system. This approach did not lead to a satisfying description of the system. Introducing 12 bends was already too much to describe the measured curve. Conflictingly the geometry of the SCB suggests the introduction of 40 bends. A comparison of measured data and a simulation with 12 implemented bends is displayed in Figure 18. The curvature of the parabolas differ. The 2-phase multiplier in Equation 3.5 had to be set to 1, otherwise an offset would have appeared as can be seen in Figure 28 in the Appendix. The difference in the curvature of the fits means a missscalling with the mass flux. This implies that one of the constants in front of the quadratic term in Equation 3.4 could have been wrongly computed.

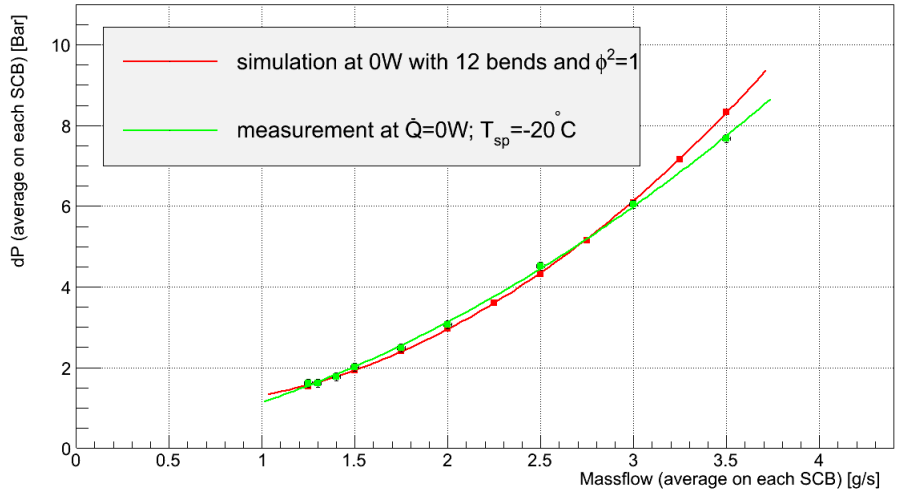

Figure 18: Comparision of a measurement at 0 W in the HERA WEST geometry and a simulation using CoBra with 10 bends and the Friedel model.

By reducing the number of bends by one, the simulation quality could not be improved, as shown in Figure 19.

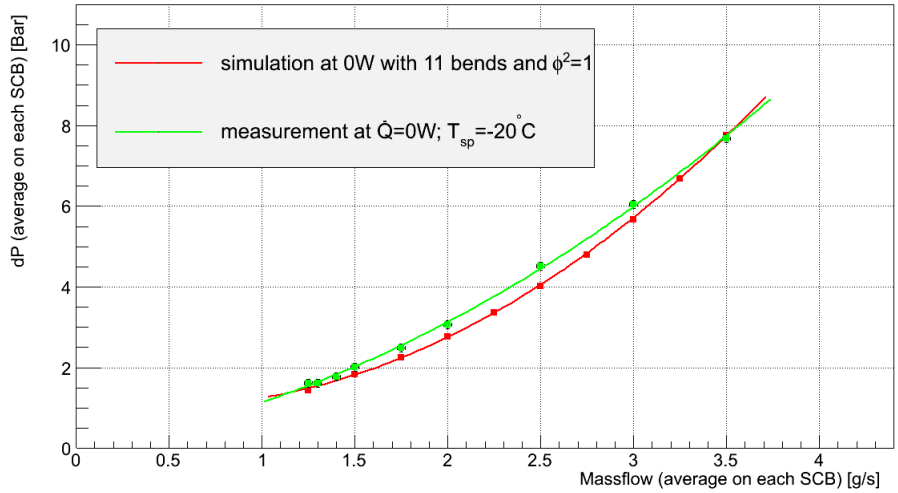

Figure 19: Comparision of a measurement at 0 W in the HERA WEST geometry and a simulation using CoBra with 11 bends and the Friedel model.

When applying heat flux the discrepancies are even more marked - see Figure 20. This suggests that this approach is not correct.

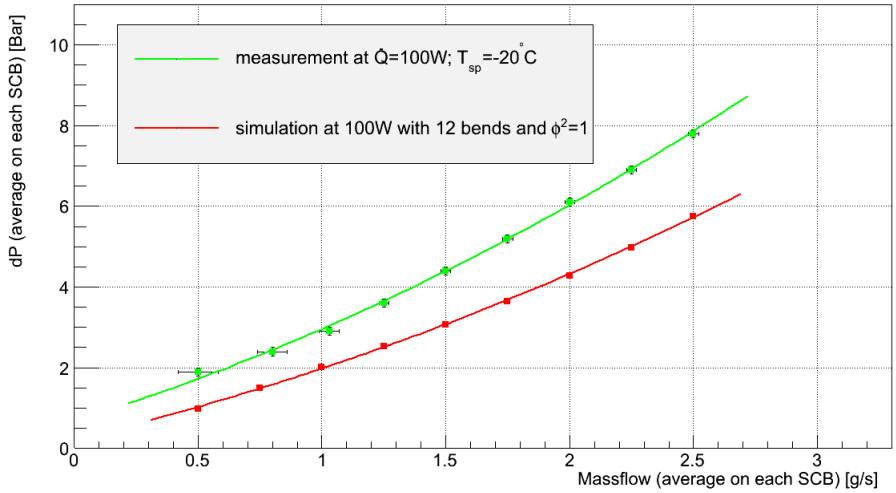

Figure 20: Comparision of a measurement at 100 W in the HERA WEST geometry and a simulation using CoBra.

Another simulation was done for the test beam setup.
The geometry is displayed in Table 3 and Figure 21.

Table 3: Test beam geometry. This geometry neglects gravitational effects because they were found to cancel each other out. See Figure 21 for a sketch of the geometry.

#	d_i [mm]	L [m]	θ [°]	Γ [W/(K·m)]
#1	6	3.6	0	0.1
#2	6	0.3	0	0.1
#3	6	0.4	0	0.1
#4	2	11.3	0	0
#5	2	0.7	0	0.5
#6	2.42	11.3	0	0
#7	6	0.4	0	0.1
#8	6	0.3	0	0.1
#9	6	0.28	0	0.1
#10	10	0.086	0	0.13
#11	9.7	0.63	0	0.13
#12	6	0.915	0	0.1
#13	6	3.3	0	0.1

A comparison of a measurement by Dipl. Ing. Reimer Stever and a simulation can be found in Figure 22. The geometry does not have a SCB. To fit the pressure drop, Equation 3.6 and 3.7 have been used to mimic valves, a distributor, effects from changing diameters and filters. Each point with a changing diameter in Table 3 has been modelled

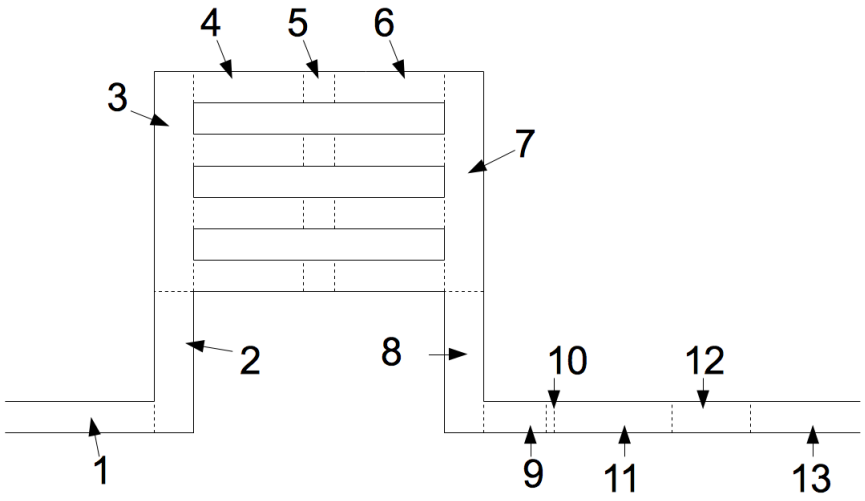

Figure 21: Sketch of the geometry as used in the test beam simulations - not to scale. Gravitational effects are ignored because they were found to cancel each other out in previous simulations. The Parameters associated with the numbers can be found in Table 3.

as such. Two filters were put in the end and the beginning of tubes 1 and end of tube 13. They were modelled as valves using Equation 3.6 where $\zeta = 5$ and $d = 0.035\,m$. These values were found to fit the curve. The heat exchange between the concentric transfer lines could not be computed because the simulations did not converge.
Another simulation without the alterations is shown in Figure 29 in the Appendix.

The pressure drop here is significantly smaller than in the HERA WEST setup although the tubes are longer. This proves that the pressure drop in the HERA WEST setup is mainly taking place in the folded SCB channel.
Some constant amount of pressure drop is still needed to fit the measured function, but it is not clear what the cause of this could be. Possible mechanisms are either the heat exchange that has not been simulated or the way the filters were modelled.
The changes in the program implemented in the second step could not be applied to the HERA WEST geometry because the numerical pressure fluctuations caused the resulting temperature to be higher than the critical temperature of CO_2. If this happens REFPROB throws an exception and the data point can not be calculated. This happens for all data points. The oscillation of the pressure drop of the last data point in the first shown simulation (Figure 18) is displayed in Figure 23. Each value depends on the previous one. If the second value is above 100 bar the exception is thrown. This suggests starting the iteration from linearly rising values and not from constant ones. It is possible that initialising the iteration with a pressure gradient of about 0.001 bar between the elements could decrease the height of the oscillations and expand the calculable parameter range.

Although the measured pressure drop could not be reproduced, single effects could be understood sufficiently. The pressure drop and resulting temperature profile of the

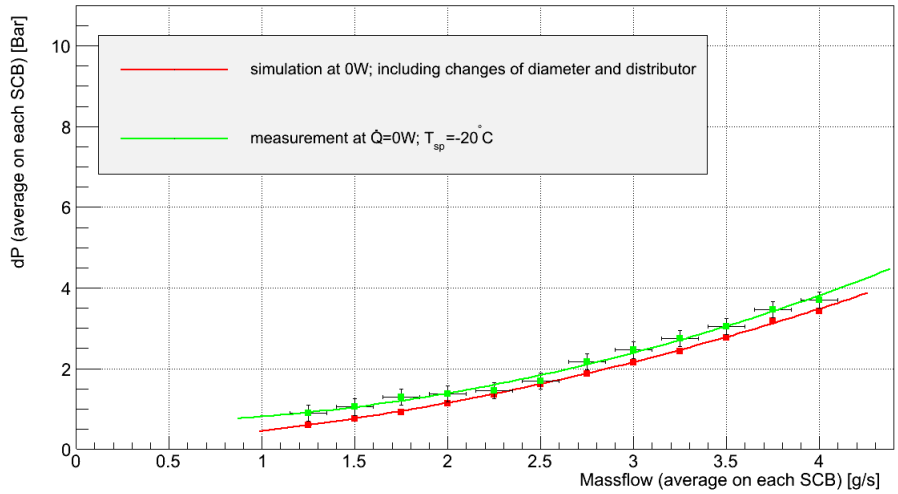

Figure 22: Comparison of a measurement and simulation in the test beam setup. The geometry used is shown in Table 3.

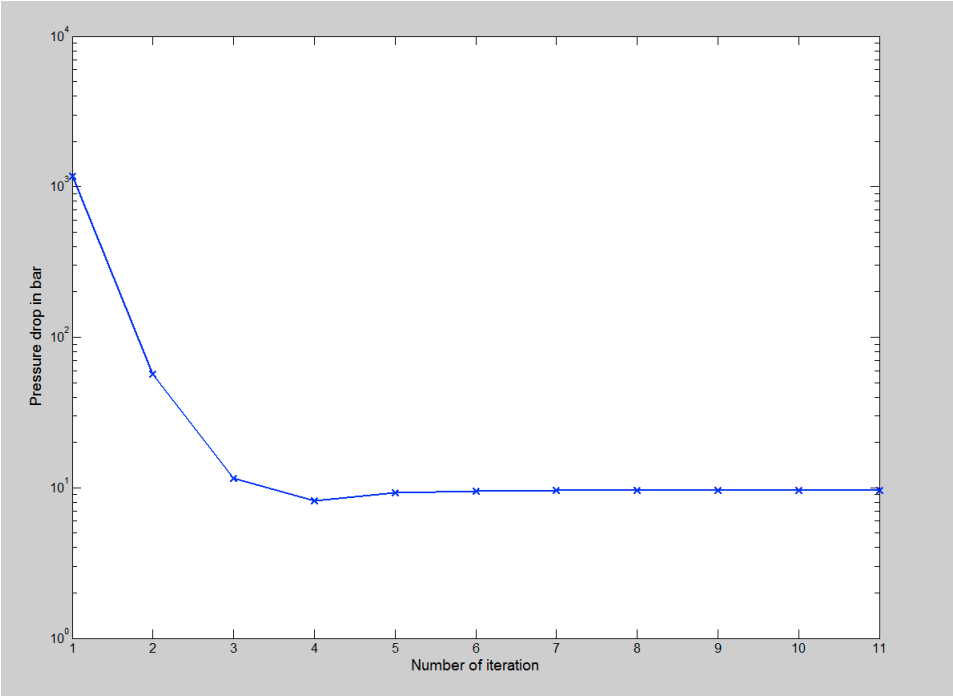

Figure 23: Graph of the numerical oscillation to the pressure drop on the HERA WEST geometry. The fourth and fifth data points are 0.02 bar lower than the subsequent points. The pressure drop is converging at 8.32 bar - the last data point in Figure 18.

HERA WEST geometry are shown in Figure 24. The tube marked A has pressure drop

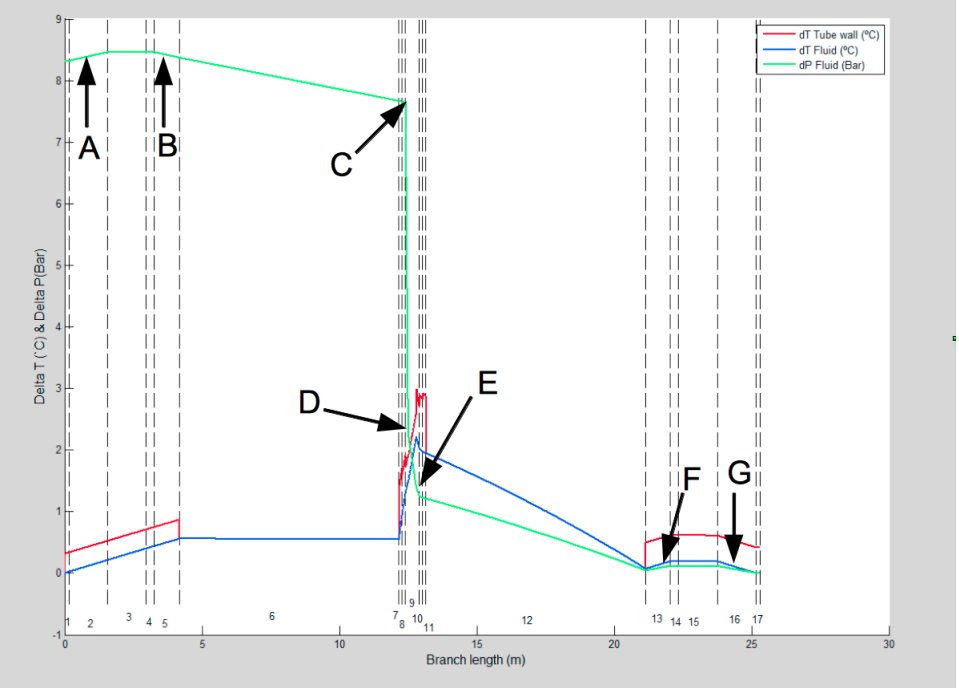

Figure 24: Pressure and temperature progression in the HERA WEST geometry in a simulation at 0 W, 3.5 g/s mass flow and 12 bends implemented. The vertically dotted lines and the numbers in-between mark the tubes as they are defined in Table 2.The characters are explain in the text below.

from gravity. This tube is ingoing and vertical, therefore the pressure is increased. In B the opposite is the case. The same is happening at F and G respectively. C and D mark the space between which the bends are implemented. The pressure is reduced by 5.25 bar in this section only. E marks the entrance into the 2-phase state.
The related enthalpy diagram is displayed in Figure 25, but as the heat flux did not scale correctly, the quality of the information is questionable.

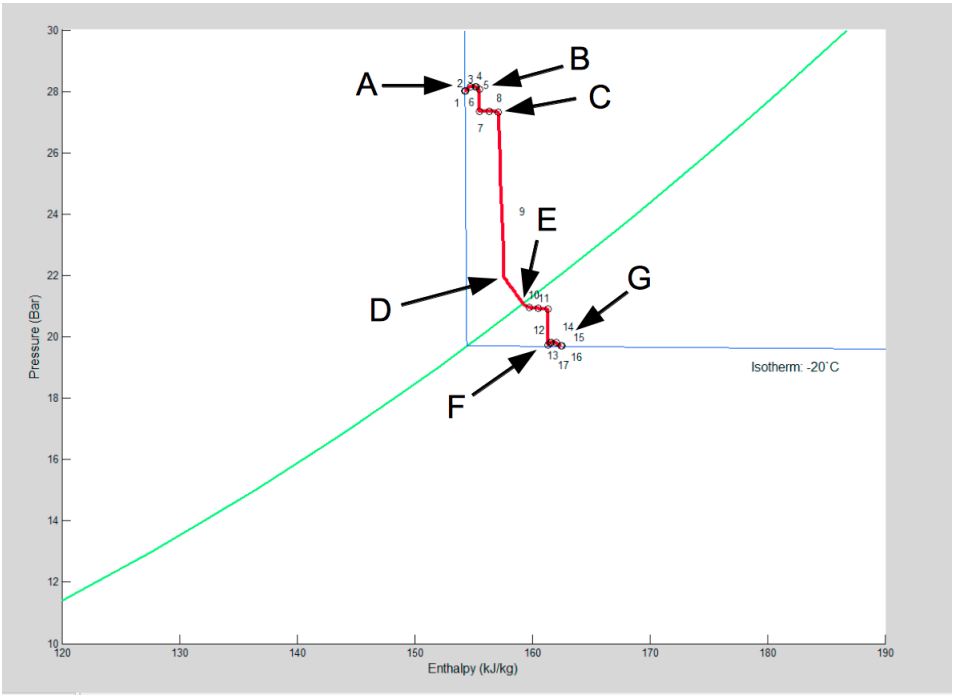

Figure 25: Enthalpy progression in the HERA WEST geometry in a simulation at 0 W, 3.5 g/s mass flow and with 12 bends implemented. The small circles and the numbers tag the tubes found in Table 2. The green line marks the 2-phase state. The blue line marks the isotherm at -20° C.

8. Conclusion

In the context of this thesis the CO_2 cooling system of the inner detector systems of Belle II was analysed. The focus was on the pressure drop characteristics of the tubes. Three measurements were conducted and produced analysable data.
The reproducibility of the SCB manufacturing standard could be verified.
The change in pressure drop with respect to the applied heat load has been measured in the HERA WEST setup. No dry out behaviour could be verified. This does not mean that no dry out occurred.
A further measurement in the test beam set up demonstrated that the main pressure drop took place in the folded channel of the SCB.
Although the measured temperature on the heated SCBs did not exceed 60° C in all configurations, it is strongly suggested that similar measurements with installed SVD cooling lines as they would appear in the detector operation in the experiment be performed.

Several simulations successfully produced data. However they failed to emulate the circumstances as they could appear in existing experiments. The quality of the simulations remains unproven, which is the reason they were only performed for the PXD systems.
In spite of these results the simulations can be used as a qualitative tool for the analysis of different geometries. The quantitative miscalling demonstrates how critical detailed measurements are to truly understand what is happening inside the tubes. However, it can be concluded that the simulations in this assignment have contributed to a better comprehension of the behaviour of the fluid and of the interaction of the tubes and fluid.
When undertaking future simulations, it is strongly advised that the numerical behaviour of CoBra be investigated. A significant advantage could be gained by switching to a faster programming environment like for example FORTRAN because the MATLAB interpreter is unsatisfactorily slow. REFPROB could be replaced by COMSOL Multiphysics when a migration to faster computing environments was intended.

References

[1] Belle II collaboration, T. Abe, *Belle II Technical Design Report*, arXiv:1011.0352 (2010).

[2] B. Verlaat, A.Colijn, *CO_2 Cooling Developments for HEP Detectors*, PoS Vertex 031 (2009) .

[3] Verlaat, B., Noite, J. *Design Considerations on long length evaporative CO_2 cooling lines*, 10^{th} IIR Gustav Lorentzen Conference on Natural Refrigerants, Delft, The Netherlands, (2012).

[4] Cheng, Lixin, Ribatski, G., Moreno Quiben, J. and Thome, J. *New prediction methods for CO_2 evaporation inside tubes: part I - a two-phase flow pattern map and a flow pattern based phenomenological model for two-phase flow frictional pressure drops*, International Journal of Heat and Mass Transfer, 51 (1-2). pp. 111-124, (2008).

[5] Cheng, Lixin, Ribatski, and Thome, J. *New prediction methods for CO_2 evaporation inside tubes: Part II - An updated general flow boiling heat transfer model based on flow patterns*, International Journal of Heat and Mass Transfer, 51(1-2). pp. 125-135, (2008).

[6] Friedel, L. *Improved friction pressure drop correlations for horizontal and vertical two phase pipe flow*, 3R Int. 18, 7, (1979).

[7] VDI-Waermeatlas, 7. Auflage, Lgb, (1994).

[8] University of Ohio *http://www.ohio.edu/mechanical/thermo/Applied/Chapt.7_11/Chapter9.html* (seen 06.01.2014).

[9] B.Verlaat, *Conceptual Design Report of MARCO*, (2011).

[10] Belle II Colaboration, *The PXD Whitebook* , (draft 2012).

[11] Belle II Colaboration, *http://belle2.kek.jp/detector.html* (seen 06.01.2014).

[12] J.G.Collier, J.R. Thome, *Convective boiling and condensation, third edition* (1994).

[13] VDI-Waermeatlas, 7. Auflage, Lc1-8, (1994).

[14] S.G.Kandlikar, *A General Correlation for Saturated two-phase flow boiling heat transfer inside horizontal and vertical tubes* J. Heat Transfer, 112(1), 219-228, (1990).

[15] CoBra, programmed by Bart Verlaat.

[16] Markus Friedel, *$https://belle2.cc.kek.jp/svn/groups/vxd\_mechanics/svd/rev0.11/full\_svd/17-01-SVD\_Assembly\_rev0.11.step$* (seen 05.02.2014).

[17] New Oxford Style Manual, Oxford University Press, ISBN 978-0-19-965722-3.

A. Appendix

A.1. Unit conversions

Parameter	Description	unit conversions
$\dot{m}$	mass flow	[kg/s]
z	coordinate of the finite element	none
T	temperature	[°C]
H	enthalpy	[J/kg]
P	pressure	[bar]
c	condition of the while loop	[J/kg]
dP	pressure drop	[bar]
V	volume of one element	[m^3]
δQ	heat uptake	[J/kg]
$\dot{Q}$	heat flow	[W]
A	surface	[m^2]
$\alpha_{\mathrm{i/o/v/wet}}$	inner/outer/vapor/wet heat transmission coefficient	[W/(K·m^2)]
L	length	[m]
$\lambda_{\mathrm{iso/t}}$	isolation/tube thermal conductivity	[W/(m·K)]
$d_{\mathrm{i/o}}$	inner/outer diameter	[m]
d_{iso}	thickness of isolation	[m]
R_{tube}	thermal resistance of the tube	[(K·m)/W]
Γ	geometry factor	[W/(m·K)]
f	friction factor	none
d_{eq}	equivalent diameter	[m]
$\rho_{\mathrm{V/L}}$	vapour/liquid density	[kg/m^3]
$u_{\mathrm{V/L}}$	vapour/liquid mean average velocity	[m/s]
x	vapour quality	none
ε	cross-sectional vapuor void fraction	none
g	gravitational acceleration	[m/s^2]
$\rho_{\mathrm{H/r}}$	homogenous/relative density	[kg/m^3]
h	heigth	[m]
θ	angle relative to earth surface	[degree]
θ_{dry}	angle of dry/wet tube perimeter	[degree]
ϕ^2	two-phase multiplier	none
ζ	pressure drop multiplier	none
Re	Reynolds Number	none
v	viscosity	[m^2/s]
Pr	Prandel Number	none

Table 4: Parameters used in the assignment.

A.2. Additional simulations

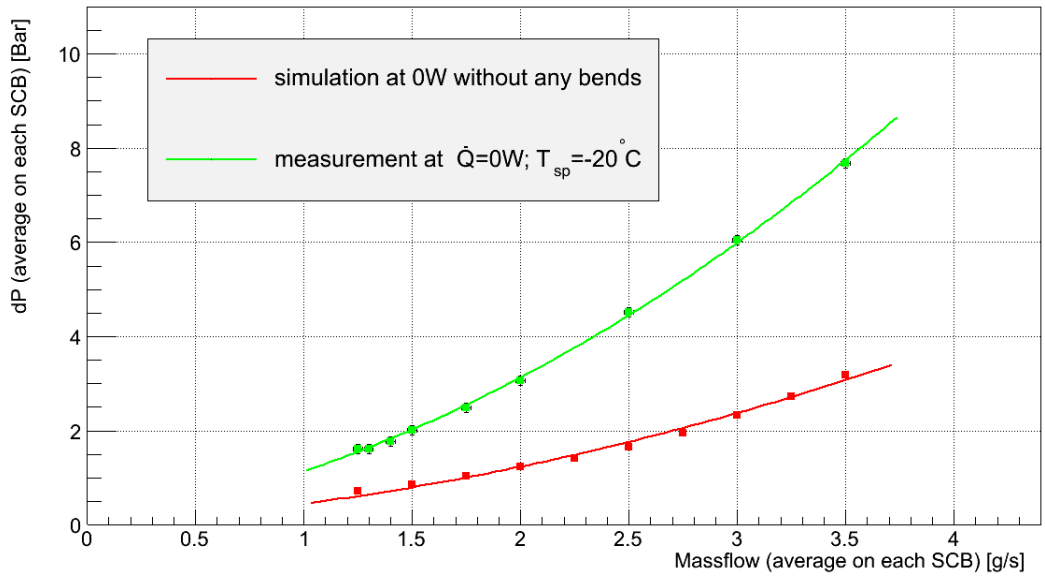

Figure 26: Comparision of a measurement at 0 W in the HERA WEST geometry and a simulation using CoBra and the Friedel model with no any alteration.

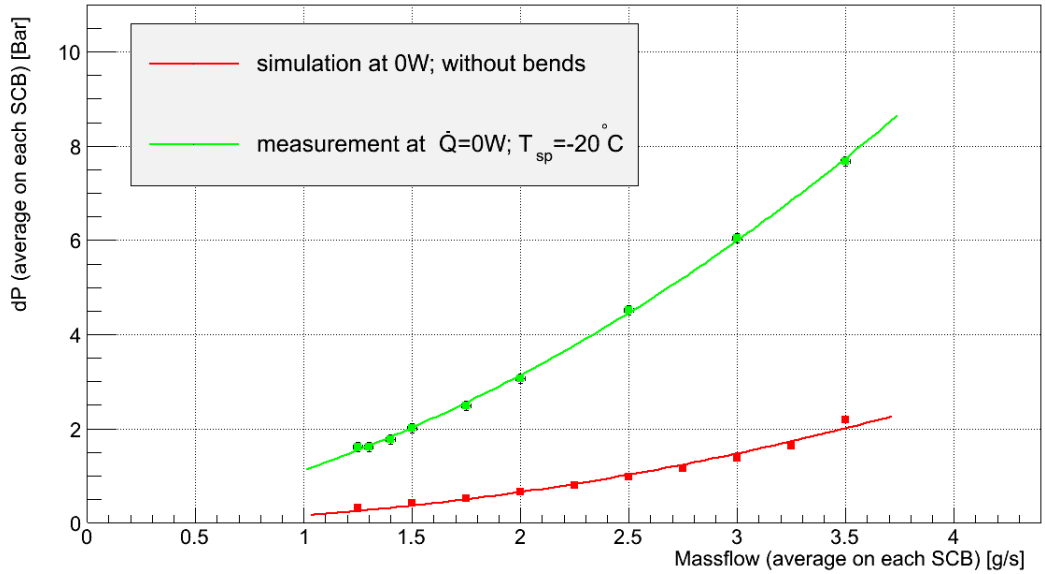

Figure 27: Comparision of a measurement at 0 W in the HERA WEST geometry and a simulation using CoBra and the Thome model with no alteration.

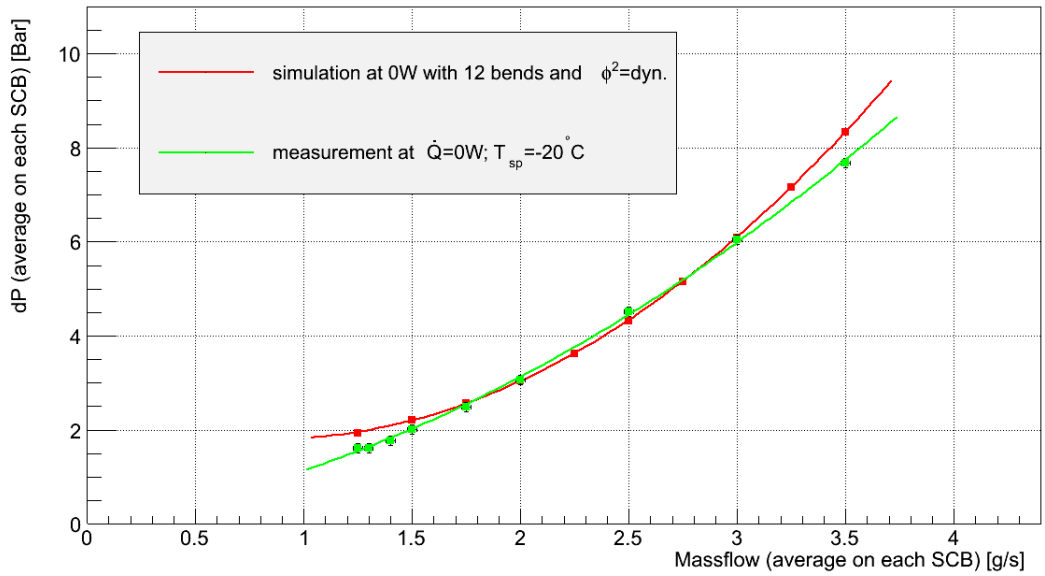

Figure 28: Comparision of a measurement at 0 W in the HERA WEST geometry and a simulation using CoBra and the Friedel model using a dynamically computed 2-phase multiplier.

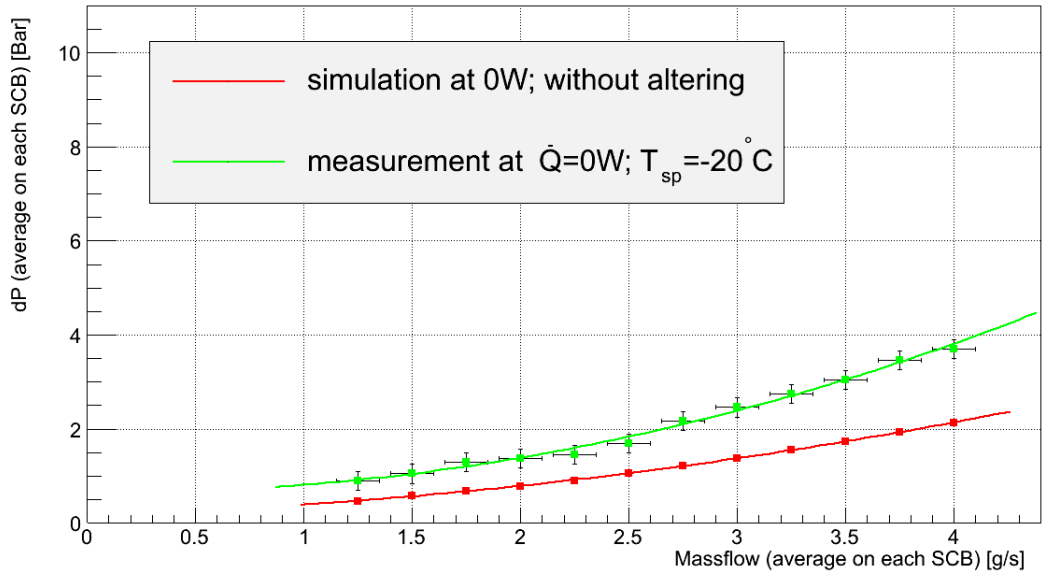

Figure 29: Comparision of a measurement at 0 W in the test beam setup with no alteration of the Friedel Model.

Erklärung

Hiermit versichere ich, dass ich diese Arbeit selbständig verfasst und keine anderen, als die angegebenen Quellen und Hilfsmittel benutzt, die wörtlich oder inhaltlich übernommenen Stellen als solche kenntlich gemacht und die Satzung der Universiät Hamburg zur Sicherung guter wissenschaftlicher Praxis in der jeweils gültigen Fassung beachtet habe.

Mit einer Veröffentlichung dieser Arbeit erkläre ich mich einverstanden.

Hamburg, den 05.02.2014

Danksagung

Ich danke Prof. Hagner und Carsten Niebuhr für die Ermöglichung dieser Arbeit. Besonders danke ich Reimer Stever für die intensive Betreuung und die Geduld mit meinen Fragen. Genauso danke ich Simon, Kim und Olli für die interessanten Gespräche und die Hilfe mit C++ bzw. ROOT.
Weiterhin möchte noch der gesamten Belle bzw. Belle II Gruppe am DESY für die schönen Monate danken!